

Long-Term Degradation Mechanisms in Application-Implemented Radical Thin Films

Ewa Malgorzata Nowik-Boltyk, Tobias Junghoefer, Mathias Glaser, Erika Giangrisostomi, Ruslan Ovsyannikov, Shuyang Zhang, Chan Shu, Andrzej Rajca, Arrigo Calzolari, and M. Benedetta Casu*



Cite This: *ACS Appl. Mater. Interfaces* 2023, 15, 30935–30943



Read Online

ACCESS |

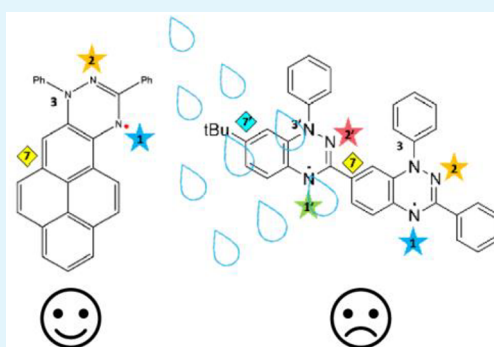
Metrics & More

Article Recommendations

Supporting Information

ABSTRACT: Blatter radical derivatives are very attractive due to their potential applications, ranging from batteries to quantum technologies. In this work, we focus on the latest insights regarding the fundamental mechanisms of radical thin film (long-term) degradation, by comparing two Blatter radical derivatives. We find that the interaction with different contaminants (such as atomic H, Ar, N, and O and molecular H₂, N₂, O₂, H₂O, and NH₂) affects the chemical and magnetic properties of the thin films upon air exposure. Also, the radical-specific site, where the contaminant interaction takes place, plays a role. Atomic H and NH₂ are detrimental to the magnetic properties of Blatter radicals, while the presence of molecular water influences more specifically the magnetic properties of the diradical thin films, and it is believed to be the major cause of the shorter diradical thin film lifetime in air.

KEYWORDS: organic radicals, Blatter radicals, thin films, photoemission, *ab initio* simulations, degradation



INTRODUCTION

New technologies need new visions and materials and, specifically, sustainable materials. In this respect, organic small molecular compounds might offer feasible routes, in consideration of factors such as raw material availability, ease of synthesis, recyclability, and their potential role in a circular economy.

Inspired by these ideas, we pioneered the controlled growth of organic radical thin films and we introduced the use of soft X-rays to investigate this class of materials.^{1,2} Materials with a radical site, i.e., with one or more unpaired electrons that give rise to a permanent magnetic moment,^{3–5} are strong candidates for ground-breaking applications,^{6–10} because of low-cost, energy saving technologies and eco-friendly production, holding the promise of social impact.^{8,11–20} While the function and performance of devices are highly important, the material stability also needs to be addressed if these technologies are to find their way to industrial applications. In this respect, we chose chemically stable organic radicals to grow thin films. We identified the properties, such as high delocalization of the unpaired electrons and high-temperature onset of the thermal degradation that give rise to films stable in ultrahigh vacuum (UHV), under X-rays, and exposed to air.^{21–24} Among the various chemically stable organic radical derivatives that are used in a variety of applications, the Blatter radical derivatives were revealed to be very successful.

In fact, the Blatter radical derivatives are very attractive due to their potential applications, ranging from batteries to

quantum technologies,^{25–33} making them a class of materials of paramount importance with the Blatter radical being an exceptionally chemically stable radical.³⁴

We have shown in previous work that the Blatter radical fulfills the necessary conditions to be evaporated without degradation, leading to chemically and thermodynamically stable thin films in ultrahigh vacuum (UHV).^{27,35} The stability is due to the large delocalization of the unpaired electron that makes it less prone to reactions.^{2,27,35} Also, we found that Blatter radical derivative thin films have a longer life when exposed to air at room temperature^{21,35} than other organic radical thin films, such as nitroxides, typically used in prototypical devices and applications.^{12,36} Although their lifetime in air is significantly long considering their radical nature, also in comparison with the known values for open and closed shell organic thin films,^{22,27,37,38} it is not indefinitely long.

Understanding (long-term) film degradation mechanisms, including their impact on the radical character and therefore on the magnetic properties, is necessary to implement the use

Received: February 13, 2023

Accepted: May 30, 2023

Published: June 15, 2023



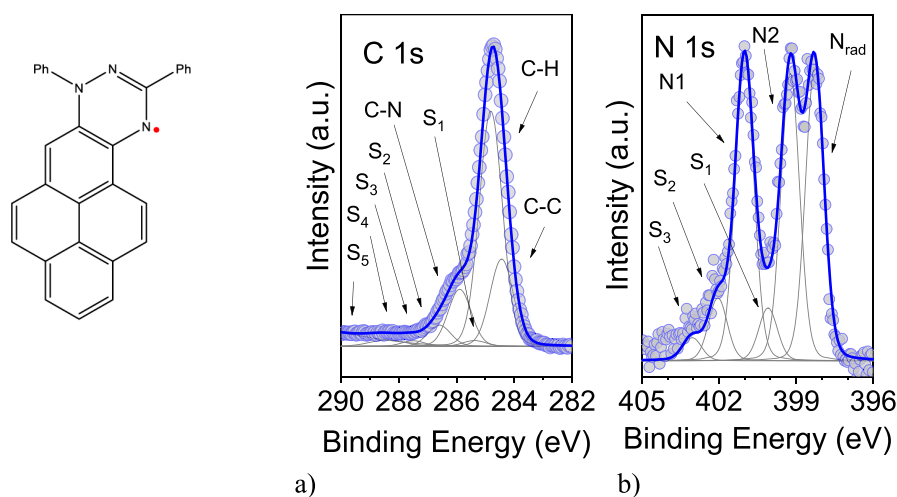


Figure 1. (Left) Molecular structure of the Blatter-pyr. C 1s (a) and N 1s (b) core level spectra of a nominally 6 nm thick film together with their fit analysis (photon energy: 1486.6 eV, for the fit parameters; see the [Supporting Information](#)).

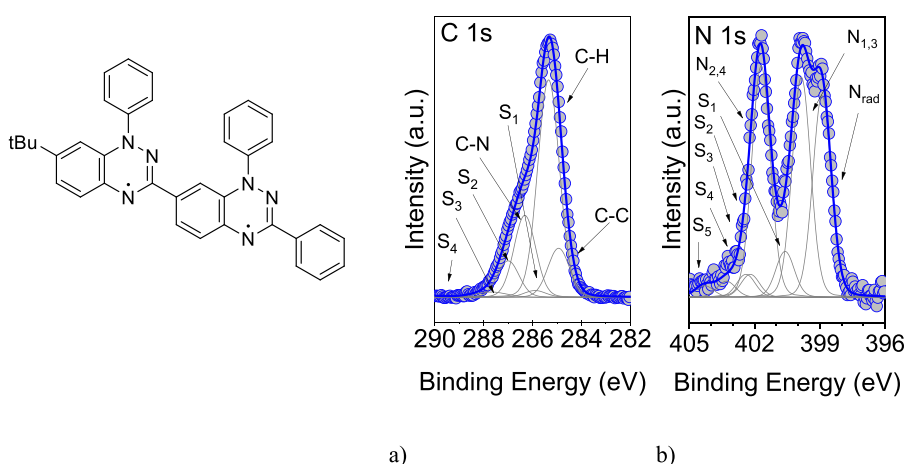


Figure 2. (Left) Molecular structure of diBlatter. C 1s (a) and N 1s (b) core level spectra of a nominally 1 nm thick film together with their fit analysis (photon energy: 1486.6 eV, for the fit parameters; see the [Supporting Information](#)).

of the Blatter radical derivatives in devices that could potentially reach the market.^{25,26,28}

In this work, we focus on the latest insights regarding the fundamental mechanisms of radical thin film degradation, by comparing two Blatter radical^{33,39} derivatives: Blatter-pyr³⁵ ($C_{29}H_{18}N_3$, [Figure 1](#)) obtained fusing a Blatter radical to a pyrene substituent, and diBlatter²¹ ($C_{36}H_{30}N_6$, [Figure 2](#)) obtained fusing two Blatter radicals. The former has one unpaired electron ($S = 1/2$), and the latter has two unpaired electrons ($S = 1$). Our work is based on a complete characterization of the long-term degradation mechanisms shown by the thin films once exposed to air, by using X-ray-based investigations, a robust fit procedure, and ab initio calculations. In particular, X-ray photoelectron spectroscopy (XPS) is a powerful analytical method that allows the monitoring of chemical changes in thin films, also when the system is made of a very small number of molecules. XPS is element-sensitive; its signal is proportional to the element concentration in the investigated systems and coupled with ab initio calculations gives a precise insight into their electronic structure. Introducing this technique to investigate radical thin films revealed its ability to identify whether the unpaired electron of the radical is involved in charge transfer, or a

chemical bond, losing its imparity and, consequently, the molecule losing its radical character.^{1,40,41}

Ours represents a general approach to investigating the degradation mechanisms in thin films, including organic and inorganic closed-shell thin films.

METHODS

Experimental Section. The Blatter-pyr and the diBlatter were synthesized as in refs 35 and 21, respectively. Film deposition and XPS measurements were performed in a UHV system consisting of a substrate preparation chamber and an organic molecular beam deposition (OMBD) dedicated chamber, connected to an analysis chamber (base pressure of $(4-9) \times 10^{-10}$ mbar) equipped with a SPECS Phoibos 150 hemispherical electron analyzer and a monochromatic Al $K\alpha$ source (SPECS Focus 500). Native SiO_2 , grown on single-side polished n-Si(111) wafers, was used as a substrate. The substrates were prepared by cleaning in ultrasonic baths of acetone and ethanol, followed by multiple cycles of annealing at around 500 K (i.e., much below the temperature at which the oxide is removed) for several hours. Their cleanliness was verified by XPS. Thin films were deposited in situ by OMBD using a Knudsen cell on the substrate kept at room temperature. The evaporation rate (evaporation rate = 0.2 nm/min) was measured with a quartz crystal microbalance, and the nominal thickness was cross-checked by using the attenuation of the XPS substrate signal (Si 2p) after the

deposition of the radical. Film characterization and stoichiometry checks were done according to refs 21 and 35. Survey and detailed XPS spectra were measured with electron pass energy of 50 and 20 eV, respectively. The binding energy scale was calibrated by using the Si 2p XPS signal (Si 2p at 99.3 eV⁴²). NEXAFS measurements were performed at the third-generation synchrotron radiation source BESSY II at the LowDosePES end station installed at the PM4 beamline ($E/\Delta E = 6000$ at 400 eV).⁴³ This end-station was equipped with a similar setup as the one described above. The same calibrated Knudsen cells, used to grow the films for the XPS measurements, were mounted to a preparation chamber attached to the NEXAFS measuring chamber to reproduce the same preparation conditions. NEXAFS spectra were measured in total electron yield and normalized with the clean substrate signal as well as the ring current. Subsequently, they were scaled to give an equal absorption edge jump.^{44,45} The reference spectra were measured on freshly prepared films. For measurements probing the film stability and lifetime after air exposure, the beam exposure was further limited, by using shorter acquisition times, to ascribe spectral changes exclusively to the degradation by air exposure. This is the reason for a worse signal-to-noise ratio in those spectra. The samples were kept under air in darkness under standard ambient temperature and pressure.

Calculation Details. Spin-unrestricted geometry optimizations for the Blatter-derived radicals were performed in the density functional theory framework by using the Quantum ESPRESSO software package.⁴⁶ All calculations employed the Perdew–Burke–Ernzerhof (PBE) exchange–correlation functional.⁴⁷ Single particle wave functions (charge) were expanded in plane waves up to a kinetic energy cutoff of 28 Ry (280 Ry). Ultrasoft pseudopotentials of the Vanderbilt type were used to simulate the ionic potentials.⁴⁸ Grimme's implementation of van der Waals corrections was included to improve the nonbonding interactions. A thick layer of vacuum (~15 Å) in the three spatial directions was included in the simulation cell to avoid spurious interactions between adjacent replicas. Each structure was fully relaxed until the forces on all atoms became lower than 0.03 eV/Å. The core level spectra were calculated in the pseudopotential framework using the final state theory.⁴⁹

RESULTS AND DISCUSSION

XPS C 1s core level spectra (Figure 1) of the thick films of Blatter-pyr are characterized by the main line at around 284.6 eV, which is attributed to photoelectrons emitted from the carbon atoms of the aromatic sites (C–C and C–H bound carbons), and a second feature at higher binding energies (285.8 eV) related to contributions from the carbon atoms bound to nitrogen atoms (C–N).³⁵ These results are mirrored by the N 1s core level spectra (Figure 1) that are characterized by three contributions that correspond to the three different nitrogen atom chemical environments, as expected for an intact Blatter-pyr.³⁵

The spectra of the diBlatter films show analogous features (Figure 2). The C 1s main line shows two distinguishable contributions. The N 1s core level spectral main features are three, as expected. They stem from the signal due to photoelectrons emitted from carbon and nitrogen atoms having a similar chemical environment as in the Blatter-pyr (compare Figures 1 and 2). The stoichiometry of the films is further proved by using a well-established fit routine,^{21,35,50} systematically correlated with electron paramagnetic resonance (EPR) results on a variety of different radicals,^{1,21,27,51–53} which indicates that all components are stoichiometrically meaningful (Tables S1–S4 in the Supporting Information). They are typical of the Blatter-pyr and diBlatter films with the expected EPR pattern corresponding to an intact (di-) radical.^{21,27,35}

Before investigating the stability of the films under air exposure, we need to define their time stability under the X-ray beam. Usually, XPS measurements are performed by scanning the sample surface to avoid radiation damage and always measuring a single spectrum on a fresh point of a freshly evaporated film. On the contrary, during this part of the experiment, we kept the beam focused on a single spot for several hours (see Supporting Information). The core level spectra do not show any evidence of chemical changes because we do not see any changes in the shape and intensity of the spectroscopy lines. After around 2 h, small changes are present (Figure S1). They can be ascribed to small morphological modifications, such as island reorganization.⁵³ This observation is also supported by the NEXAFS spectra that confirm the high stability of the films under the beam exposure with only minor changes in the intensity indicating small structural adjustments under the beam (Figures S2 and S3). The beam stability of the films is a prerequisite to investigating the film lifetime under air exposure without artifacts due to potential radiation damage.

We exposed the films to air keeping them at room temperature (Figures 3 and S4). The C 1s core level spectra

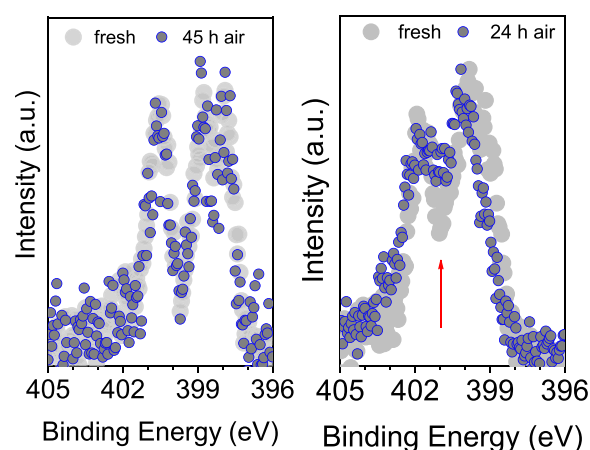


Figure 3. N 1s core level spectra before (light gray) and after (bluish) air exposure for thin films of Blatter-pyr (left panel, after 45 h in air) and diBlatter (right panel, after 24 h in air) (photon energy: 1486.6 eV). The arrow indicates the increased intensity in the 400–401 eV range upon air exposure.

are less prone to major changes (Figure S4). It is also interesting to note that there are no new features due to the possible oxidation of the Blatter radicals,⁵⁴ as observed in solution using either MnO₂ or KMnO₄ as oxidant.³⁴ The occurrence of a double bond between a carbon atom and an oxygen atom would give rise to an additional feature in the higher binding energy range, i.e., immediately following the C–N component. This feature is not present in our spectra (Figures 4 and S4). For this oxidation pattern to occur, the C7 carbon atom must be such that its position makes a bond with oxygen favorable, as in the Blatter radical.³⁴ It is sufficient to block it, and the Blatter radical stability toward oxidation is strongly enhanced.³⁴ In this work, the Blatter-pyr is protected, the Blatter radical being fused to the pyrene, and the diBlatter is protected by a *tert*-butyl group and the second Blatter radical.

Looking at the C 1s core level spectra, we note that diBlatter thin films show changes on a shorter time scale than the Blatter-pyr thin films (Figure S4). Those changes pertain to the

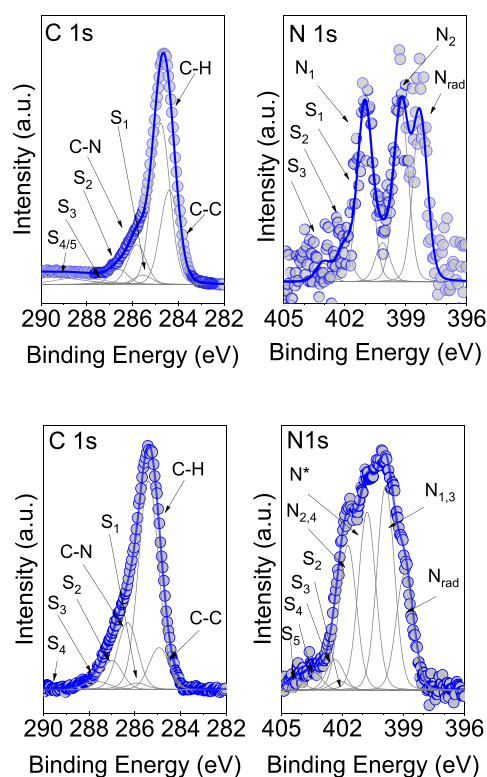


Figure 4. C 1s and N 1s core level spectra together with their fits after air exposure for thin films of Blatter-pyr (upper panel, after 45 h) and diBlatter (lower panel, after 72 h in air) (photon energy: 1486.6 eV, for the fit parameters; see the Supporting Information).

second feature at higher binding energies related to the carbon atoms bound to nitrogen atoms. Indeed, the N 1s core level spectra reveal clear changes (Figures 3 and 4). N 1s core level spectra are particularly important for the systems under investigation because they carry the information on the unpaired electrons and therefore on the radical character of the films, which is of interest for the goal of the present work. We observe changes in the shape of the N 1s core level curves for both Blatter-pyr and diBlatter thin films, although on a different time scale, as found for the C 1s core level spectra.

Electron paramagnetic resonance (EPR) spectroscopy investigations have shown that Blatter-pyr films are stable for up to three months under air³⁵ and diBlatter for at least 18 h.²¹ Therefore, we have especially focused on the diBlatter thin films N 1s core level spectra, monitoring them and comparing the results to those obtained for the Blatter-pyr thin films. This enables understanding the chemical mechanisms playing a role and their impact on the thin film properties and assessing the role of the two radical sites versus one.

The major change that is observed is that the characteristic dip (at around 400 eV) between the first two components and the third one is progressively canceled within 24 h (see the arrow in Figure 3, right panel) and disappears after 72 h in diBlatter thin films, replaced by the increased signal intensity in this binding energy range (the N* feature in Figure 4). This is concomitant with the decrease of the signal of the first feature (Nrad) at lower binding energy (see also the fit parameters in the Supporting Information) that is correlated with the radical character of the films.^{21,27,35} Blatter-pyr films show only a very small increase in intensity in the same binding energy range

after 1 week in air.³⁵ This feature also emerges when evaporation is not fully successful.⁴⁰

These results indicate the coexistence of two ongoing phenomena: (1) the new N* signal indicates a change in the chemical environment of the nitrogen atoms, and (2) a certain percentage of molecules have lost their radical character. This can be estimated by using the fit analysis comparing the relative fit contributions before and after air exposure. In the diBlatter films, the loss is around 38% after 72 h (see Tables S4 and S8). Note that we do not have any information on how the first satellite feature (S₁) might change under air exposure; thus, in the fit, we consider its intensity in N*.

The intensity in the binding energy range of N* is typically correlated with chemical interactions due to the hydrogenation or oxidation of the nitrogen atoms.⁴² For example, a bond between oxygen and the nitrogen atom that emits photoelectrons contributing to the Nrad feature would move the binding energy of the photoemitted electrons to the higher binding energy range leading to an increased intensity where N* is identified. Also, the presence of molecular water might give rise to similar effects on the N 1s core level signals. Considering the oxidation pattern of the Blatter radical in solution,^{34,34} we would exclude the occurrence of a bond between nitrogen atoms and oxygen in the Blatter radical derivatives investigated in this work.

To shed further light on the impact of air exposure on the electronic structure and the radical character of the two systems, we have performed ab initio calculations.

Air in the atmosphere is mostly composed of nitrogen, oxygen, argon, noble gases, and molecular water. By using simulations from first-principles, we considered the effect of the most relevant elements (H, Ar, N, O) and molecules (H₂, N₂, O₂, OH, H₂O, NH₂) that can react/adsorb on the radical films during air exposure. Several other gases and molecules, which stem from human activities, may be present, too, in urban environments (e.g., pollution).⁵⁵ The study of these contaminants goes beyond the aim of this work.

Because of the critical role of nitrogen in the Blatter radical derivatives, we considered different adsorption sites on the radical (S_i, with *i* = 1, 2, 1', 2', Figure 5). All adsorbed atoms and molecules are in their neutral charge state. For each radical, atom/molecule, and adsorption site, we fully relaxed

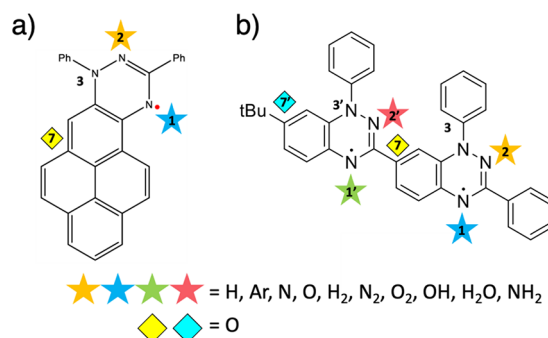


Figure 5. Sketch of selected impurities included in the calculations for (a) Blatter-pyr and (b) diBlatter. Numerical labels identify the chemically different nitrogen atoms within the molecules (N₁, N₂, N₁', N₂'). Colored symbols mark the adsorption sites and the adsorbed molecular species: stars indicate atoms/molecules attached to radical nitrogens (N_i), and diamonds indicate oxygen attached to carbon site C₇ or C₇'.

the atomic structure, and we studied the resulting electronic and magnetic properties. The results are summarized in Tables 1 and 2, where we reported the magnetic moment (μ) for the

Table 1. Magnetic Moment (μ) and Formation Energy (ΔE_f) of Blatter-pyr upon Adsorption of Characteristic Elements (H, H⁺, Ar, N, O) and Molecules (H₂, N₂, O₂, OH, H₂O, NH₂) Present in Air in Standard Conditions as a Function of the Adsorption Sites (S_i)^a

★/◆	Blatter-pyr		
	site	μ (Bohr mag)	ΔE_f (eV)
H	S1	0.00	−0.80
	S2	0.00	−0.29
H ⁺	S1	1.00	
	S2	1.00	
Ar	S1	1.00	0.00
	S2	1.00	0.00
N	S1	0.00	+2.59
	S2	0.00	+1.62
O	S1	1.00	−0.20
	S2	1.00	−0.19
	C7	1.00	+0.15
H ₂	S1	1.00	0.00
	S2	1.00	0.00
N ₂	S1	1.00	0.00
	S2	1.00	0.00
O ₂	S1	1.00	0.00
	S2	1.00	0.00
OH	S1	0.00	+1.75
	S2	0.00	+1.57
H ₂ O	S1	1.00	−0.37
	S2	1.00	−0.33
NH ₂	S1	0.00	−1.40
	S2	0.00	−1.38

^aLabels and symbols refer to Figure 5. Boldfaced areas indicate energetically unfavored adsorption configurations.

final systems, along with the formation energy (ΔE_f) calculated as $\Delta E_f = E_{\text{tot}} - E_{\text{rad}} - E_{\text{mol}}$, where E_{tot} is the ground state total energy after the impurity adsorption, E_{rad} is the total energy of the pristine radical, and E_{mol} is the total energy of the attached molecule.

In the case of Blatter-pyr, the adsorption of H, O, H₂O, and NH₂ is energetically favored, while the reaction is unfavored in the case of the atomic N and the OH fragment. We can thus exclude these two contaminant agents from those that have the highest probability to cause film degradation. The S1 adsorption site is generally energetically more favorable than the S2 one (see Figure 5 and Table 1). Noble gas (Ar) and divalent molecules (H₂, N₂, O₂) do not react with the radical (i.e., $\Delta E_f = 0$) moving away from the starting S_i sites and leaving the electronic and magnetic properties of the radical unperturbed (see Figure S5, Supporting Information). This excludes also these elements/molecules from the possible degradation causes. Among the interacting and energetically favored impurities, the inclusion of H, and NH₂ quenches the magnetic moment of the radical, restoring the double electron pairing. This is due to the formation of N–H bonds between atom N₁ or N₂ of the radical (depending on the adsorption site) and the contaminant H or NH₂. This saturates the initial charge unbalance, as demonstrated by the density of state (DOS) plot shown in Figure S5 of the Supporting Information.

Table 2. Magnetic Moment (μ) and Formation Energy (ΔE_f) of diBlatter upon Adsorption of Characteristic Elements and Molecules Present in Air in Standard Conditions as a Function of the Adsorption Sites (S_i)^a

★/◆	diBlatter		
	site	μ (Bohr mag)	ΔE_f (eV)
H	S1	1.00	−0.80
	S2	1.00	−0.32
	S1'	1.00	−0.80
	S2'	1.00	−0.33
Ar	S1	2.00	0.00
	S2	2.00	0.00
	S1'	2.00	0.00
	S2'	2.00	0.00
N	S1	1.00	+2.46
	S2	1.00	+1.73
	S1'	1.00	+2.51
	S2'	1.00	+1.79
O	S1	2.00	−0.37
	S2	1.00	+0.03
	S1'	2.00	−0.36
	S2'	1.00	−0.01
H ₂	C7	2.00	+0.72
	C7'	0.00	−0.01
	S1	2.00	0.00
	S2	2.00	0.00
N ₂	S1	2.00	0.00
	S2	2.00	0.00
	S1'	2.00	0.00
	S2'	2.00	0.00
O ₂	S1	2.00	0.00
	S2	2.00	0.00
	S1'	2.00	0.00
	S2'	2.00	0.00
OH	S1	1.00	+1.79
	S2	1.00	+1.62
	S1'	1.00	+1.81
	S2'	1.00	+1.60
H ₂ O	S1	0.00	−0.40
	S2	2.00	−0.25
	S1'	0.00	−0.25
	S2'	0.00	−0.22
NH ₂	S1	1.00	−1.46
	S2	1.00	−1.36
	S1'	1.00	−1.43
	S2'	1.00	−0.40

^aLabels and symbols refer to Figure 5. Boldfaced areas indicate energetically unfavored adsorption configurations.

Different is the case of the O-based impurities (O and H₂O). Atomic oxygen forms covalent N–O bonds as well as H-bonds with the surrounding H atoms. This explains the energy gain upon adsorption. Yet, oxygen does not change the dipole moment of the radical because of the unpaired N–O electrons. In the case of H₂O, we do not find the formation of covalent bonds as for the other systems but of O–H...N hydrogen bonds between water and the radical. As a result, the radical maintains its initial spin configuration.

The different initial charge state of the impurities (i.e., ionized/radical impurities) could change the degradation effect

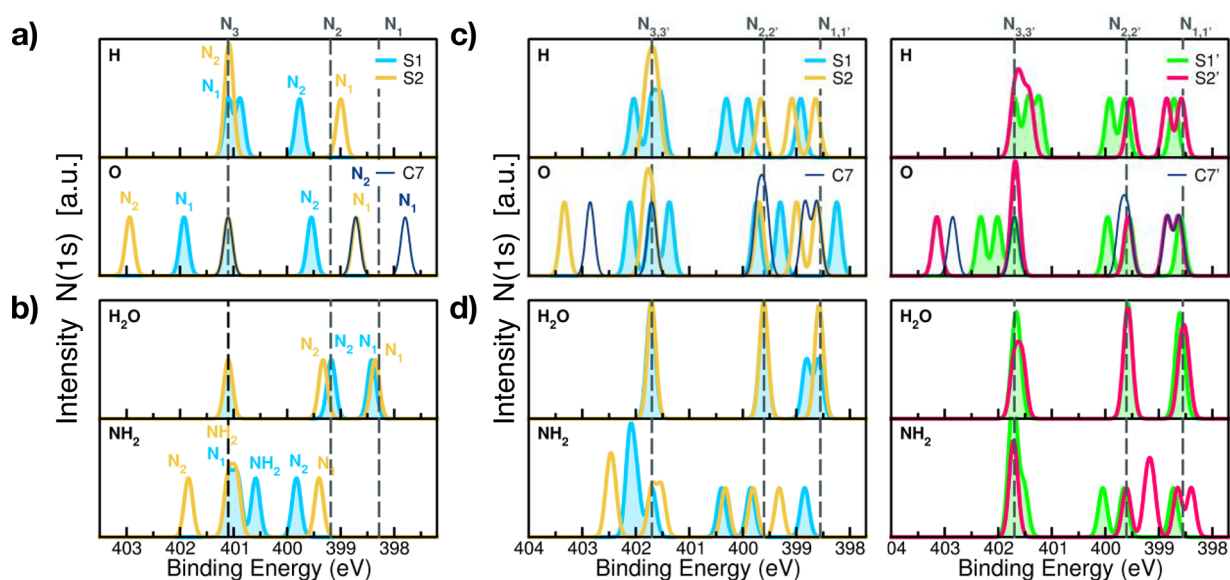


Figure 6. Simulated N 1s core level spectra of (a, b) Blatter-pyr and (c, d) diBlatter upon adsorption of characteristic (a, c) atoms (H, O) and (b, d) molecules (H_2O , NH_2) and as a function of the adsorption sites S1, S2, and C7 for Blatter-pyr and S1, S1', S2, S2', C7, and C7' for diBlatter. Vertical dashed lines refer to the core-level features of the pristine molecules. The N_3 peak is assumed as the energy reference for all spectra and aligned to the experimental value for a direct comparison. Labels and colors refer to Figure 5.

on the radicals, as it modifies the total electron distribution of the system. For example, the adsorption of H^+ proton leaves the radical unperturbed (Table 1), since the lack of the valence electron impedes the electron pairing that quenches the magnetic moment, as in the case of the neutral H discussed above (Figure S5, Supporting Information).

Qualitatively similar results also hold for diBlatter: molecular contaminant adsorption is energetically favored in the case of H, O, H_2O , and NH_2 , while it is unfavored in the case of atomic N and OH. S1 and S1' sites are slightly more stable than the corresponding S2, and S2' ones. The formation energies of equivalent sites on the two radical units (S1/S1' and S2/S2') are very similar but not identical as the diBlatter is not structurally symmetric. The adsorption of H, N, OH, or NH_2 saturates one of the two unpaired electrons, reducing the magnetic moment from two to one (i.e., total spin reduction from $S = 1$ to $S = 1/2$). Again, oxygen and water behave differently. When adsorbed in S1 and S1', oxygen forms energetically stable bonds, but it does not change the magnetic moment of the radical, as for the Blatter-pyr case. When attached to S2 and S2', the energy gain is negligible; thus the relative deterioration of the moment of the molecule ($\mu = 1.0$ Bohr mag) is thermodynamically unfavored.

In the case of water, although no covalent bonds are formed, the polarization effect due to the formation of H-bonds with the radical imparts an internal charge redistribution that couples and pairs the originally unpaired electron, zeroing the magnetic moment of the molecule ($\mu = 0$). This is confirmed by the DOS plot shown in Figure S6 (see the Supporting Information). In only one case (H_2O at S2) this polarization seems to be less effective, and the molecule maintains its initial spin. DiBlatter radical is not sensitive to the presence of Ar and diatomic molecules (H_2 , N_2 , O_2).

Atomic H and NH_2 molecules seem to have the same degradation effect on both radicals. Conversely, from the different interactions of Blatter-pyr and diBlatter with molecular water, we can infer that molecular water may have a stronger degradation effect on diBlatter thin films, causing

the difference in film lifetime between Blatter-pyr and diBlatter films when exposed to air.

To investigate the possible formation of quinone terminations and their effect on the magnetic properties of the molecule, we further considered the adsorption of atomic O at C7 and C7'. In the former case, the adsorption is energetically unfavored for both radicals; adsorption in C7' (for diBlatter only) is only slightly favored. The difference is due to the inequivalent atomic environment between C7 and C7' which are connected to a phenyl or a butyl group, respectively. This agrees with the experimental observation that the formation of C–O bonds is not favored and, in general, atomic oxygen is not a source of magnetic degradation for these systems.

To have a direct comparison with the experimental data, we simulated the N 1s core level spectra after molecule adsorption, as shown in Figure 6. Panels a and c report the results for atomic H and O species, and panels b and d report those for H_2O , and NH_2 molecules.

Since the approach we used provides only the relative shift between the core level binding energies of inequivalent atoms, here we shifted the simulated spectra to the experimental value of the N_3 peaks of each radical (i.e., 401.1 eV for Blatter-pyr and 401.7 eV for diBlatter) for a direct comparison. The calculated spectra of both radicals have a three-peaked shape, where each peak is associated with the three inequivalent nitrogen atoms of the molecules (see Figures 1, 2, and 5). The numerical values (Blatter-pyr, $\text{N}_1 = 398.3$ eV, $\text{N}_2 = 399.2$ eV, $\text{N}_3 = 401.1$ eV; diBlatter, $\text{N}_{1,1}' = 401.1$ eV, $\text{N}_2 = 399.6$ eV, $\text{N}_{3,3}' = 398.6$ eV) are in excellent agreement with the experimental values and are marked as vertical dashed lines in Figure 6. The adsorption of contaminants modifies this plot, shifting the energy position of the peak as a function of the attached species and the adsorption site. Specifically, the adsorption of contaminants in position S1 gives rise, for both Blatter-pyr and diBlatter, to intensity in the binding energy range around 400–401 eV, as experimentally observed with XPS (Figures 3 and 4). Water, which weakly interacts with radicals, hardly modifies the original spectra. The adsorption of the other investigated

element/molecules is energetically unfavored or has a neutral effect on the radicals; thus, they do not contribute significantly to the modification of the XPS spectra (Figure S7 in the Supporting Information). In particular, diatomic molecules and noble gas do not modify the three characteristic peaks of the Blatter radicals. Even though the adsorption of H^+ does not modify the magnetic properties of the radicals, it changes the local environment of the bonded nitrogen. This effect is detectable in the simulated XPS spectra. Yet, the low percentage of H^+ ions in air is expected to give a minor contribution to the experimental spectra. OH adsorption would generate a major degradation effect on the radicals, imparting relevant changes to the XPS spectra. However, the thermodynamical analysis does not predict this type of reaction, confirming the experimental findings.

This variety of contributions is the origin of the additional intensity and line broadening observed in the experimental spectra upon air exposure. Therefore, these features are the spectroscopic indication of the degradation of the magnetic properties of the radicals when they are exposed to air, that is, when exposed to molecular contaminant attaching/adsorption.

CONCLUSIONS

Stability and degradation mechanisms in materials that are candidates for new applications are of foremost importance. Our work focuses on the degradation mechanisms upon air exposure in two Blatter radical derivatives.

Our multitechnique investigations indicate that the Blatter radical derivative films are chemically very stable; however, they are affected by long-term degradation. In our previous work on understanding why diradical evaporation is challenging, we observed that the number of radical sites makes a difference. Also when comparing the same radical in a single or diradical configuration, the diradical evaporation is always more complicated.²² We obtain analogous results comparing the film lifetime of Blatter-pyr and diBlatter in the present work.

We analyzed the degradation effect due to the adsorption of most chemical elements and molecules present in air. On a general ground, the long-term stability of Blatter radicals is justified by the low/selective reactivity to most air components. We found that the adsorption of contaminants such as H , H_2O , and NH_2 is energetically favorable, while noble gases and diatomic molecules do not react with radicals. For H , and NH_2 , adsorption on both radical and diradical derivatives leads to the quenching of the pristine magnetic moment.

Our work indicates that the interaction with different contaminants affects the chemical and magnetic properties of the thin films upon air exposure but also the chemical structure of the radicals is important: the adsorption of contaminants on different sites affects the core levels in different ways.

Our calculations indicate that molecular water also plays a role; because we found that Blatter-pyr is molecular water resistant while diBlatter is not, diBlatter films degrade in a shorter time. From the experimental point of view, techniques such as near ambient pressure XPS, currently in development also in the soft X-ray range, allowing exposure in UHV of the investigated surface to selected gases or contaminants, including vapor and liquid water, are new opportunities to be pursued to further deepen the comprehension of these degradation patterns. Molecular water is ubiquitously present also in clean environments for device production. The

presence of “intrinsic” molecular water is known to play a role in the degradation mechanisms in organic devices, such as organic light-emitting devices,⁵⁶ and hybrid perovskite-based devices.⁵⁷ Showing that Blatter-pyr is resistant in the presence of molecular water is a key result for the use of the Blatter radical in real devices.

ASSOCIATED CONTENT

Supporting Information

The Supporting Information is available free of charge at <https://pubs.acs.org/doi/10.1021/acsami.3c02057>.

XPS fit parameters for the freshly evaporated films, time-dependent core level signals, time-dependent NEXAFS signals, C 1s core level spectra after air exposure, XPS fit parameters after air exposure, spin polarized density of states of the Blatter-pyr, spin polarized density of states (DOS) of the diBlatter, simulated N 1s core level spectra of Blatter-pyr upon adsorption of characteristic H^+ , H_2 , Ar, and OH species and as a function of the adsorption sites (S1) (PDF)

AUTHOR INFORMATION

Corresponding Author

M. Benedetta Casu – *Institute of Physical and Theoretical Chemistry, University of Tübingen, 72076 Tübingen, Germany*; orcid.org/0000-0002-5659-7040;
Email: benedetta.casu@uni-tuebingen.de

Authors

Ewa Malgorzata Nowik-Boltyk – *Institute of Physical and Theoretical Chemistry, University of Tübingen, 72076 Tübingen, Germany*; orcid.org/0000-0003-3136-4870

Tobias Junghoefer – *Institute of Physical and Theoretical Chemistry, University of Tübingen, 72076 Tübingen, Germany*

Mathias Glaser – *Institute of Physical and Theoretical Chemistry, University of Tübingen, 72076 Tübingen, Germany*

Erika Giangrisostomi – *Institute Methods and Instrumentation for Synchrotron Radiation Research, Helmholtz-Zentrum Berlin, 12489 Berlin, Germany*

Ruslan Ovsyannikov – *Institute Methods and Instrumentation for Synchrotron Radiation Research, Helmholtz-Zentrum Berlin, 12489 Berlin, Germany*

Shuyang Zhang – *Department of Chemistry, University of Nebraska, Lincoln, Nebraska 68588, United States*

Chan Shu – *Department of Chemistry, University of Nebraska, Lincoln, Nebraska 68588, United States*

Andrzej Rajca – *Department of Chemistry, University of Nebraska, Lincoln, Nebraska 68588, United States*;
orcid.org/0000-0002-8856-1536

Arrigo Calzolari – *CNR-NANO Istituto Nanoscienze, 41125 Modena, Italy*; orcid.org/0000-0002-0244-7717

Complete contact information is available at:
<https://pubs.acs.org/doi/10.1021/acsami.3c02057>

Author Contributions

E.M.N.-B., T.J., M.G., E.G., R.O., and M.B.C. performed the measurements. S.Z., C.S., and A.R. designed and synthesized the radicals. A.C. performed the calculations. E.M.N.-B. and T.J. performed the fits. M.B.C. conceived and supervised the project, interpreted the experimental data, and wrote the

manuscript together with A.C. All authors contributed to the discussion and commented on the manuscript.

Notes

The authors declare no competing financial interest.

The data that support the findings of this study are available from the corresponding author upon reasonable request.

ACKNOWLEDGMENTS

The authors thank Helmholtz-Zentrum Berlin (HZB) for providing beamtime at BESSY II, E. Nadler for technical support, and Dr. M. Pink for the X-ray structures of the radicals. Financial support from HZB and the German Research Foundation (DFG, Contract CA852/11-3, Project Number 394233453) is gratefully acknowledged. The authors thank the Chemistry Division of the National Science Foundation for supporting this research under Grants CHE-1665256 and CHE-1955349 (A.R.). Computer resources were provided by the TACC supercomputing center (TX, USA) through QUANTRANS project. This work was partly supported by the European Union's Horizon 2020 Research and Innovation program under Grant Agreement 965046, FET-Open Project Interfast (Gated INTERfaces for FAST information processes).

REFERENCES

- (1) Casu, M. B. Nanoscale Studies of Organic Radicals: Surface, Interface, and Spinterface. *Acc. Chem. Res.* **2018**, *51* (3), 753–760.
- (2) Junghoefer, T.; Calzolari, A.; Baev, I.; Glaser, M.; Ciccullo, F.; Giangrisostomi, E.; Ovsyannikov, R.; Kielgast, F.; Nissen, M.; Schwarz, J.; Gallagher, N. M.; Rajca, A.; Martins, M.; Casu, M. B. Magnetic behavior in metal-free radical thin films. *Chem* **2022**, *8* (3), 801–814.
- (3) Epifanov, G. I. *Solid State Physics*; Mir Publisher: Moscow, 1979.
- (4) Gatteschi, D.; Sessoli, R.; Villain, J. *Molecular Nanomagnets*; Oxford University Press Inc.: New York, 2006.
- (5) Getzlaff, M. *Fundamentals of Magnetism*; Springer-Verlag: Berlin, 2008.
- (6) Nakazawa, S.; Nishida, S.; Ise, T.; Yoshino, T.; Mori, N.; Rahimi, R. D.; Sato, K.; Morita, Y.; Toyota, K.; Shiomi, D.; Kitagawa, M.; Hara, H.; Carl, P.; Höfer, P.; Takui, T. A Synthetic Two-Spin Quantum Bit: g-Engineered Exchange-Coupled Biradical Designed for Controlled-NOT Gate Operations. *Angew. Chem., Int. Ed.* **2012**, *51* (39), 9860–9864.
- (7) Sproules, S. Molecules as electron spin qubits. In *Electron Paramagnetic Resonance: Volume 25*; The Royal Society of Chemistry, 2017; pp 61–97.
- (8) Oyaizu, K.; Nishide, H. Radical Polymers for Organic Electronic Devices: A Radical Departure from Conjugated Polymers? *Adv. Mater.* **2009**, *21* (22), 2339–2344.
- (9) Suga, T.; Konishi, H.; Nishide, H. Photocrosslinked nitroxide polymer cathode-active materials for application in an organic-based paper battery. *Chem. Commun.* **2007**, No. 17, 1730–1732.
- (10) Wasielewski, M. R.; Forbes, M. D. E.; Frank, N. L.; Kowalski, K.; Scholes, G. D.; Yuen-Zhou, J.; Baldo, M. A.; Freedman, D. E.; Goldsmith, R. H.; Goodson, T.; Kirk, M. L.; McCusker, J. K.; Ogilvie, J. P.; Shultz, D. A.; Stoll, S.; Whaley, K. B. Exploiting chemistry and molecular systems for quantum information science. *Nat. Rev. Chem.* **2020**, *4* (9), 490–504.
- (11) Domingo, N.; Bellido, E.; Ruiz-Molina, D. Advances on structuring, integration and magnetic characterization of molecular nanomagnets on surfaces and devices. *Chem. Soc. Rev.* **2012**, *41* (1), 258–302.
- (12) Lee, J.; Lee, E.; Kim, S.; Bang, G. S.; Shultz, D. A.; Schmidt, R. D.; Forbes, M. D. E.; Lee, H. Nitronyl Nitroxide Radicals as Organic Memory Elements with Both n- and p-Type Properties. *Angew. Chem., Int. Ed.* **2011**, *50* (19), 4414–4418.
- (13) Simão, C.; Mas-Torrent, M.; Crivillers, N.; Lloveras, V.; Artés, J. M.; Gorostiza, P.; Veciana, J.; Rovira, C. A robust molecular platform for non-volatile memory devices with optical and magnetic responses. *Nat. Chem.* **2011**, *3* (5), 359–364.
- (14) Tomlinson, E. P.; Hay, M. E.; Boudouris, B. W. Radical Polymers and Their Application to Organic Electronic Devices. *Macromolecules* **2014**, *47* (18), 6145–6158.
- (15) Huskinson, B.; Marshak, M. P.; Suh, C.; Er, S.; Gerhardt, M. R.; Galvin, C. J.; Chen, X.; Aspuru-Guzik, A.; Gordon, R. G.; Aziz, M. J. A metal-free organic-inorganic aqueous flow battery. *Nature* **2014**, *505* (7482), 195–198.
- (16) Crivillers, N.; Mas-Torrent, M.; Rovira, C.; Veciana, J. Charge transport through unpaired spin-containing molecules on surfaces. *J. Mater. Chem.* **2012**, *22* (28), 13883–13890.
- (17) Sugawara, T.; Komatsu, H.; Suzuki, K. Interplay between magnetism and conductivity derived from spin-polarized donor radicals. *Chem. Soc. Rev.* **2011**, *40* (6), 3105–3118.
- (18) Davis, R. M.; Sowers, A. L.; DeGraff, W.; Bernardo, M.; Thetford, A.; Krishna, M. C.; Mitchell, J. B. A novel nitroxide is an effective brain redox imaging contrast agent and in vivo radioprotector. *Free Radical Biol. Med.* **2011**, *51* (3), 780–790.
- (19) Sowers, M. A.; McCombs, J. R.; Wang, Y.; Paletta, J. T.; Morton, S. W.; Dreaden, E. C.; Boska, M. D.; Ottaviani, M. F.; Hammond, P. T.; Rajca, A.; Johnson, J. A. Redox-responsive branched-bottlebrush polymers for in vivo MRI and fluorescence imaging. *Nat. Commun.* **2014**, *5*, 5460.
- (20) Rajca, A.; Wang, Y.; Boska, M.; Paletta, J. T.; Olanikitwanit, A.; Swanson, M. A.; Mitchell, D. G.; Eaton, S. S.; Eaton, G. R.; Rajca, S. Organic Radical Contrast Agents for Magnetic Resonance Imaging. *J. Am. Chem. Soc.* **2012**, *134* (38), 15724–15727.
- (21) Zhang, S.; Pink, M.; Junghoefer, T.; Zhao, W.; Hsu, S.-N.; Rajca, S.; Calzolari, A.; Boudouris, B. W.; Casu, M. B.; Rajca, A. High-Spin ($S = 1$) Blatter-Based Diradical with Robust Stability and Electrical Conductivity. *J. Am. Chem. Soc.* **2022**, *144* (13), 6059–6070.
- (22) Junghoefer, T.; Gallagher, N. M.; Kolanji, K.; Giangrisostomi, E.; Ovsyannikov, R.; Chassé, T.; Baumgarten, M.; Rajca, A.; Calzolari, A.; Casu, M. B. Challenges in controlled thermal deposition of organic diradicals. *Chem. Mater.* **2021**, *33*, 2019–2028.
- (23) Shu, C.; Pink, M.; Junghoefer, T.; Nadler, E.; Rajca, S.; Casu, M. B.; Rajca, A. Synthesis and Thin Films of Thermally Robust Quartet ($S = 3/2$) Ground State Triradical. *J. Am. Chem. Soc.* **2021**, *143*, 5508–5518.
- (24) Calzolari, A.; Rajca, A.; Casu, M. B. From radical to triradical thin film processes: the Blatter radical derivatives. *J. Mater. Chem. C* **2021**, *9* (33), 10787–10793.
- (25) Ji, Y.; Long, L.; Zheng, Y. Recent advances of stable Blatter radicals: synthesis, properties and applications. *Mater. Chem. Front.* **2020**, *4* (12), 3433–3443.
- (26) Zhang, Y.; Zheng, Y.; Zhou, H.; Miao, M.-S.; Wudl, F.; Nguyen, T.-Q. Temperature Tunable Self-Doping in Stable Diradicaloid Thin-Film Devices. *Adv. Mater.* **2015**, *27* (45), 7412–7419.
- (27) Ciccullo, F.; Calzolari, A.; Bader, K.; Neugebauer, P.; Gallagher, N. M.; Rajca, A.; van Slageren, J.; Casu, M. B. Interfacing a Potential Purely Organic Molecular Quantum Bit with a Real-Life Surface. *ACS Appl. Mater. Interfaces* **2019**, *11* (1), 1571–1578.
- (28) Zheng, Y.; Miao, M.-s.; Dantelle, G.; Eisenmenger, N. D.; Wu, G.; Yavuz, I.; Chabinyk, M. L.; Houk, K. N.; Wudl, F. A Solid-State Effect Responsible for an Organic Quintet State at Room Temperature and Ambient Pressure. *Adv. Mater.* **2015**, *27* (10), 1718–1723.
- (29) Häupler, B.; Schubert, U. S.; Wild, A.; Koutentis, P. A.; Zissimou, G. Verwendung benzotriazinyl-haltiger Polymere als Ladungsspeicher. Patent DE102017005924 (A1), Dec 27, 2018.
- (30) Steen, J. S.; Nuismier, J. L.; Eiva, V.; Wiglema, A. E. T.; Daub, N.; Hjelm, J.; Otten, E. Blatter Radicals as Bipolar Materials for Symmetrical Redox-Flow Batteries. *J. Am. Chem. Soc.* **2022**, *144* (11), 5051–5058.
- (31) Saal, A.; Elbinger, L.; Schreyer, K.; Fataj, X.; Friebe, C.; Schubert, U. S. Structural Improvement of the Blatter Radical for

- High-Current Organic Batteries. *ACS Appl. Energy Mater.* **2022**, *5* (12), 15019–15028.
- (32) Poryvaev, A. S.; Gjuzi, E.; Yazikova, A. A.; Polyukhov, D. M.; Albrekht, Y. N.; Efreimov, A. A.; Kudriavkikh, N. A.; Yanshole, V. V.; Hoffmann, F.; Fröba, M.; Fedin, M. V. Blatter Radical-Decorated Silica as a Prospective Adsorbent for Selective NO Capture from Air. *ACS Appl. Mater. Interfaces* **2023**, *15* (4), 5191–5197.
- (33) Constantinides, C. P.; Berezin, A. A.; Manoli, M.; Leitun, G. M.; Zissimou, G. A.; Bendikov, M.; Rawson, J. M.; Koutentis, P. A. Structural, Magnetic, and Computational Correlations of Some Imidazolo-Fused 1,2,4-Benzotriazinyl Radicals. *Chem.—Eur. J.* **2014**, *20* (18), 5388–5396.
- (34) Constantinides, C. P.; Koutentis, P. A.; Krassos, H.; Rawson, J. M.; Tasiopoulos, A. J. Characterization and Magnetic Properties of a “Super Stable” Radical 1,3-Diphenyl-7-trifluoromethyl-1,4-dihydro-1,2,4-benzotriazin-4-yl. *J. Org. Chem.* **2011**, *76* (8), 2798–2806.
- (35) Ciccullo, F.; Gallagher, N. M.; Geladari, O.; Chasse, T.; Rajca, A.; Casu, M. B. A Derivative of the Blatter Radical as a Potential Metal-Free Magnet for Stable Thin Films and Interfaces. *ACS Appl. Mater. Interfaces* **2016**, *8* (3), 1805–1812.
- (36) Poggin, L.; Cucinotta, G.; Sorace, L.; Caneschi, A.; Gatteschi, D.; Sessoli, R.; Mannini, M. Nitronyl nitroxide radicals at the interface: a hybrid architecture for spintronics. *Rendiconti Lincei. Scienze Fisiche e Naturali* **2018**, *29* (3), 623–630.
- (37) Tesi, L.; Lucaccini, E.; Cimatti, I.; Perfetti, M.; Mannini, M.; Atzori, M.; Morra, E.; Chiesa, M.; Caneschi, A.; Sorace, L.; Sessoli, R. Quantum coherence in a processable vanadyl complex: new tools for the search of molecular spin qubits. *Chem. Sci.* **2016**, *7* (3), 2074–2083.
- (38) Maliakal, A.; Raghavachari, K.; Katz, H.; Chandross, E.; Siegrist, T. Photochemical Stability of Pentacene and a Substituted Pentacene in Solution and in Thin Films. *Chem. Mater.* **2004**, *16* (24), 4980–4986.
- (39) Blatter, H. M.; Lukaszewski, H. A new stable free radical. *Tetrahedron Lett.* **1968**, *9* (22), 2701–2705.
- (40) Low, J. Z.; Kladnik, G.; Patera, L. L.; Sokolov, S.; Lovat, G.; Kumarasamy, E.; Repp, J.; Campos, L. M.; Cvetko, D.; Morgante, A.; Venkataraman, L. The Environment-Dependent Behavior of the Blatter Radical at the Metal–Molecule Interface. *Nano Lett.* **2019**, *19* (4), 2543–2548.
- (41) Ajayakumar, M. R.; Moreno, C.; Alcón, I.; Illas, F.; Rovira, C.; Veciana, J.; Bromley, S. T.; Mugarza, A.; Mas-Torrent, M. Neutral Organic Radical Formation by Chemisorption on Metal Surfaces. *J. Phys. Chem. Lett.* **2020**, *11* (10), 3897–3904.
- (42) Moulder, J. F. *Handbook of X-ray Photoelectron Spectroscopy*; Perkin-Elmer Corp., 1992.
- (43) Giangrisostomi, E.; Ovsyannikov, R.; Sorgenfrei, F.; Zhang, T.; Lindblad, A.; Sassa, Y.; Cappel, U. B.; Leitner, T.; Mitzner, R.; Svensson, S.; Mårtensson, N.; Föhlich, A. Low Dose Photoelectron Spectroscopy at BESSY II: Electronic structure of matter in its native state. *J. Electron Spectrosc. Relat. Phenom.* **2018**, *224*, 68–78.
- (44) Casu, M. B.; Cosseddu, P.; Batchelor, D.; Bonfiglio, A.; Umbach, E. A high-resolution near-edge x-ray absorption fine structure investigation of the molecular orientation in the pentacene/poly(3,4-ethylenedioxythiophene):poly(styrenesulfonate) pentacene/system. *J. Chem. Phys.* **2008**, *128* (1), 014705.
- (45) Casu, M. B. Nanoscale Order and Structure in Organic Materials: Diindenoperylene on Gold as a Model System. *Cryst. Growth Des.* **2011**, *11* (8), 3629–3635.
- (46) Giannozzi, P.; Baroni, S.; Bonini, N.; Calandra, M.; Car, R.; Cavazzoni, C.; Ceresoli, D.; Chiarotti, G. L.; Cococcioni, M.; Dabo, I.; Dal Corso, A.; de Gironcoli, S.; Fabris, S.; Fratesi, G.; Gebauer, R.; Gerstmann, U.; Gougoussis, C.; Kokalj, A.; Lazzeri, M.; Martin-Samos, L.; Marzari, N.; Mauri, F.; Mazzarello, R.; Paolini, S.; Pasquarello, A.; Paulatto, L.; Sbraccia, C.; Scandolo, S.; Sclauzero, G.; Seitsonen, A. P.; Smogunov, A.; Umari, P.; Wentzcovitch, R. M. Quantum ESPRESSO: a modular and open-source software project for quantum simulations of materials. *J. Phys.: Condens. Matter* **2009**, *21* (39), 395502.
- (47) Perdew, J. P.; Burke, K.; Ernzerhof, M. Generalized Gradient Approximation Made Simple. *Phys. Rev. Lett.* **1996**, *77* (18), 3865–3868.
- (48) Vanderbilt, D. Soft self-consistent pseudopotentials in a generalized eigenvalue formalism. *Phys. Rev. B* **1990**, *41* (11), 7892–7895.
- (49) Pehlke, E.; Scheffler, M. Evidence for site-sensitive screening of core holes at the Si and Ge (001) surface. *Phys. Rev. Lett.* **1993**, *71* (14), 2338–2341.
- (50) Junghoefer, T.; Nowik-Boltyk, E. M.; de Sousa, J. A.; Giangrisostomi, E.; Ovsyannikov, R.; Chassé, T.; Veciana, J.; Mas-Torrent, M.; Rovira, C.; Crivillers, N.; Casu, M. B. Stability of radical-functionalized gold surfaces by self-assembly and on-surface chemistry. *Chem. Sci.* **2020**, *11* (34), 9162–9172.
- (51) Kakavandi, R.; Ravat, P.; Borozdina, Y. B.; Baumgarten, M.; Casu, M. B. Electronic Structure and Stability of Fluorophore–Nitroxide Radicals from Ultrahigh Vacuum to Air Exposure. *ACS Appl. Mater. Interfaces* **2015**, *7* (3), 1685–1692.
- (52) Kakavandi, R.; Savu, S.-A.; Sorace, L.; Rovai, D.; Mannini, M.; Casu, M. B. Core-Hole Screening, Electronic Structure, and Paramagnetic Character in Thin Films of Organic Radicals Deposited on SiO₂/Si(111). *J. Phys. Chem. C* **2014**, *118* (15), 8044–8049.
- (53) Savu, S.-A.; Biswas, I.; Sorace, L.; Mannini, M.; Rovai, D.; Caneschi, A.; Chassé, T.; Casu, M. B. Nanoscale Assembly of Paramagnetic Organic Radicals on Au(111) Single Crystals. *Chem.—Eur. J.* **2013**, *19* (10), 3445–3450.
- (54) Neugebauer, F. A.; Umminger, I. Über 1,4-Dihydro-1,2,4-benzotriazinyl-Radikale. *Chem. Ber.* **1980**, *113* (4), 1205–1225.
- (55) Schlesinger, W. H.; Bernhardt, E. S. The Atmosphere. In *Biogeochemistry*, 4th ed.; Schlesinger, W. H., Bernhardt, E. S., Eds.; Academic Press, 2020; Chapter 3, pp 51–97.
- (56) Scholz, S.; Kondakov, D.; Lüssem, B.; Leo, K. Degradation Mechanisms and Reactions in Organic Light-Emitting Devices. *Chem. Rev.* **2015**, *115* (16), 8449–8503.
- (57) Deretzis, I.; Smecca, E.; Mannino, G.; La Magna, A.; Miyasaka, T.; Alberti, A. Stability and Degradation in Hybrid Perovskites: Is the Glass Half-Empty or Half-Full? *J. Phys. Chem. Lett.* **2018**, *9*, 3000–3007.